Flow and transport in a pleated filter

Cite as: Phys. Fluids **34**, 097102 (2022); https://doi.org/10.1063/5.0102940 Submitted: 13 June 2022 • Accepted: 08 August 2022 • Published Online: 07 September 2022

Daniel Fong and (ii) Pejman Sanaei









Physics of Fluids

Special Topic: Hydrogen Flame and Detonation Physics

Submit Today!

Flow and transport in a pleated filter

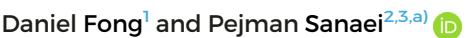
Cite as: Phys. Fluids **34**, 097102 (2022); doi: 10.1063/5.0102940 Submitted: 13 June 2022 · Accepted: 8 August 2022 · Published Online: 7 September 2022







•



AFFILIATIONS

- ¹Department of Mathematics and Science, U.S. Merchant Marine Academy, Kings Point, New York 11024, USA
- ²Department of Mathematics, New York Institute of Technology, New York, New York 10023, USA
- ³Department of Mathematics and Statistics, Georgia State University, Atlanta, Georgia 30303, USA

ABSTRACT

A pleated membrane filter consists of a porous membrane layer, which is surrounded by two supporting layers, and the whole structure is pleated and placed into a cylindrical cartridge. Pleated membrane filters are used in a variety of industrial applications, since they offer more surface area to volume ratio that is not found in equivalent flat filters. In this work, we introduce a novel three-dimensional model of a pleated membrane filter that consists of an empty region, a pleated region, and a hollow region. The advection diffusion equation is used to model contaminant concentration in the membrane pores along with Darcy's law to model the flow within the membrane and support layers, while the Stokes equation is used for the flow in the empty region and the hollow region. We further use the key assumptions of our model based on small aspect ratios of the filter cartridge and the pleated membrane to simplify the governing equations, which can be easily solved by numerical methods. By performing these steps, we seek to discover an optimal pleat packing density to find the optimum filter performance, while not exceeding a threshold for the particle concentration at the filter outlet.

Published under an exclusive license by AIP Publishing. https://doi.org/10.1063/5.0102940

I. INTRODUCTION

At the most fundamental level, filtration is the process of passing a fluid through a porous medium in order to remove unwanted particles from the feed solution. ¹⁻⁴ The porous layers of media in a filter are known as membranes, which are responsible for the separation of contaminants from a fluid feed solution. Performance of a filter can be affected by many different factors such as the internal structure of the membrane and the membrane pore geometry. The porous membrane of a filter gradually becomes fouled as the separation of particles from the fluid takes place and this results in a higher resistance to the flow. To compensate for the increase in resistance, more energy or a higher pressure gradient is needed in the system. The most common and typical fouling mechanisms are adsorption, complete blocking, intermediate blocking, and cake formation, which have been studied by many researchers until now. ^{1,5-8}

Membrane filters—essentially, thin sheets of a porous medium which act as filters—find widespread use for filtration applications such as water treatment, various purification processes in the biotech industry, 2,9-11 removing impurities from the blood in kidney dialysis, 12,13 and beer clarification. 14,15 Other applications include fruit juice processing, 16 recycling micro-organism, 17 and enhanced oil recovery, 18 among many others. 19 Here, we expand on a couple of these

applications. The process of extracting crude oil and other natural resources from the earth often results in an abundance of impurities such as suspended solids, oil, and sulfides being present in the extracted resource.²⁰ The mining of crude oil can be performed in different ways, from horizontal and vertical drilling, to hydraulic fracturing. Regardless of the method of extracting the crude oil, the process includes several steps, one of which includes utilizing pleated filtration systems to get rid of the impurities present.²⁰ The global demand for water resources has led to an immoderate exploitation of our resources resulting in dangerous amounts of wastewater being emitted into our environment. Some examples of industrial applications that generate these copious amounts of wastewater are the textile industries and the vegetable oil refinery process. In the process of treating, oil and water mixtures, conventional methods such as biological treatments, gravitational separation, and dissolved air flotation all prove to be insufficient. Membrane filtration has proven to be a useful alternative in the oil refinery process because of the advantageous characteristics membrane filter possess such as easy separation, efficient oil removal, and low energy costs, to name a few. Utilizing membrane filtration for oil refinery has its weaknesses, however; one main disadvantage that may arise while utilizing a membrane filtration system to treat oil mixtures is fouling. Over the filter's life cycle, particles and other impurities will

^{a)}Author to whom correspondence should be addressed: psanaei@gsu.edu. URL: https://sites.google.com/view/pejman-sanaeis-webpage

accumulate and result in a higher resistance in the system. Fouling makes a filtration system more costly because of the materials needed for cleaning the membrane and in some cases replace the entirety of the membrane filter. ^{21,22}

Pleated membrane filters are a type of filter in which the filter media are pleated, commonly around a cylindrical cartridge in order to provide a high amount of surface filtration area. They are widely used in fields such as virus removal,²³ air ventilation systems,²⁴ agriculture,²⁵ nuclear air filtration,²⁶ pulse-jet cleaning,²⁷ and wastewater treatment.²⁸ Cylindrical pleated membrane filter cartridges at the most basic level consist of an empty region surrounding a pleated membrane region as well as a hollow region at the center for outflow. They are designed so that a fluid can enter the pleated membrane radially from an outside inlet and once filtered, exit out of the cartridge from its hollow region at the outlet. The pleated membrane is also supported by two additional porous layers on either side, known as the support layers, which are more thicker, porous and as by design, they are not meant to capture particles over time. 29,30 Together, each of these three layers are pleated and packed along the cartridge to form a pleated membrane region that filters impurities from the fluid. Pleated filters are unique in the way that their high surface area to volume ratio is much higher than flat non-pleated membrane filters with equivalent surface area.³¹ Larger membrane surface area yields benefits such as lower flux (which increases capacity and lifespan) and smaller housings, which are less expensive, take less time to manufacture, and are easier to handle from lower steaming and cooling times. 23,32 However, the performance of a pleated membrane filter is inferior when compared to a flat unpleated with the same membrane surface area.^{29,3} This stems from several factors such as the additional resistance to the overall system due to the pleat packing density as well as the support layers and the complex fluid dynamics within the pleated membrane. This raises the question of how to optimize the filter cartridge geometry and the pleat packing density in such a way that the filter yields maximum performance.

Recent works^{29,30,34} attempted only to answer the part of the above question using simplified models that focused on a two-dimensional flow as well as solely advective particle transport flow through the membrane. As a result, the models did not include any variation along the filter cartridge axial direction, and the effects of contaminants diffusion were neglected. Practically, in a slow filtration process, or during the late stages of filtration when the flow rate is naturally very low due to a high level of fouling, particle diffusion could play an important role.^{35,36}

In this paper, we develop a mathematical model that caters for the mentioned extensions by including two additional regions as shown in Figs. 1(a) and 1(b): (a) the empty region, where the flow enters the cartridge and then passes into the pleated region; and (b) the hollow region, which is a central hollow duct for outflow. We model the flow within these two regions by the Stokes equations in axisymmetric cylindrical coordinates. In our investigation, we focus on pleated filters with high pleat packing density (PPD), so that the air gaps between adjacent pleats are assumed to be insignificant. For the pleated region, which consists of a membrane and two support layers, we distinguish the support layers from the membrane by incorporating cylindrical coordinates with angular dependency. The flow in the support layers is modeled by Darcy's law, while the Stokes equation in axisymmetric cylindrical coordinates is used to model the flow within

the membrane internal pores. The flow equations within these five regions will be simplified by using asymptotic analysis based on the small aspect ratios of the membrane and cartridge.

In addition, we consider the mass transport of the diluted particles in the feed through the membrane. The fouling occurs within the membrane; therefore, its performance deteriorates with time and, as a result, the membrane permeability decreases. The flow equations within the membrane described above are coupled to the advection-diffusion equation for the contaminant transport and then simplified by asymptotic analysis using the small aspect ratios of membrane pore geometry. The results are used to optimize the filter pleat packing density in order to maximize the pleated membrane filter performance based on the total amount of filtered fluid and the retention rate.

This paper is organized as follows: in Sec. II, we introduce a mathematical model for the pleated membrane regions and describe the filter cartridge geometry. In Sec. III, the governing equations of flow and transport are introduced. In Sec. IV, we introduce appropriate scalings for the flow regimes of interest as well as particle transport to nondimensionalize the models from Sec. III. Then, in Sec. V, we use asymptotic analysis based on the filter cartridge and the pleated membrane region small aspect ratios to simplify the governing equations introduced in Sec. IV. Afterwards, we present a summary of our models and a numerical method to solve them in Sec. VI. Then, we show the results of simulations that address filtration performance; specifically, the particle retention and the amount of filtrate fluid are calculated and analyzed in Sec. VII. Finally, we conclude and summarize our modeling results in Sec. VIII and provide some insight into real-world applications as well.

II. MATHEMATICAL DESCRIPTION

We consider the transport of fluid (or solute) through a cylindrical pleated filter cartridge with characteristic height L. A typical pleated filter cartridge consists of an empty region, a pleated region, and a central hollow region of radii R_e , R_m , and R_h , respectively. We assume R_e , R_m , $R_h \ll L$, $\epsilon_m = R_m/L \ll 1$ and set $d = (R_e - R_m)/R_m$. As illustrated in Fig. 1(a), the flow enters from the bottom of the empty region and then moves into the pleated region to be filtered and finally exits out of the bottom of the hollow region. We use an axisymmetric cylindrical coordinate system (r, θ, z) to represent the filtration flow problem in the empty region and hollow region, where r, θ , and z denote the radial, azimuth, and axial directions, respectively. Figure 1(b) shows the cross-sectional view of the cylindrical pleated filter in Fig. 1(a). The flow in the pleated region is more complicated and should be modeled more carefully as discussed below.

The pleated region consists of a membrane and two porous support layers. As mentioned in the introduction, we restrict our attention to pleated filters with tightly packed pleats (high PPD); such that we may assume that the membrane region is occupied by either a porous support material or a membrane with no air gaps. To further simplify the geometry, we consider pleated membrane filters composed of an identical array of uniformly distributed pleats around the entire filter cartridge. Figure 1(c) illustrates what a single pleat would look like in a cylindrical pleated filter while Fig. 1(d) indicates how the geometry is idealized in our model by neglecting the folded part of the membrane and assuming symmetry about the centerline of the pleat. The flow enters the outer support layer from the empty region and then passes through the membrane and leaves the inner support layer to exit out

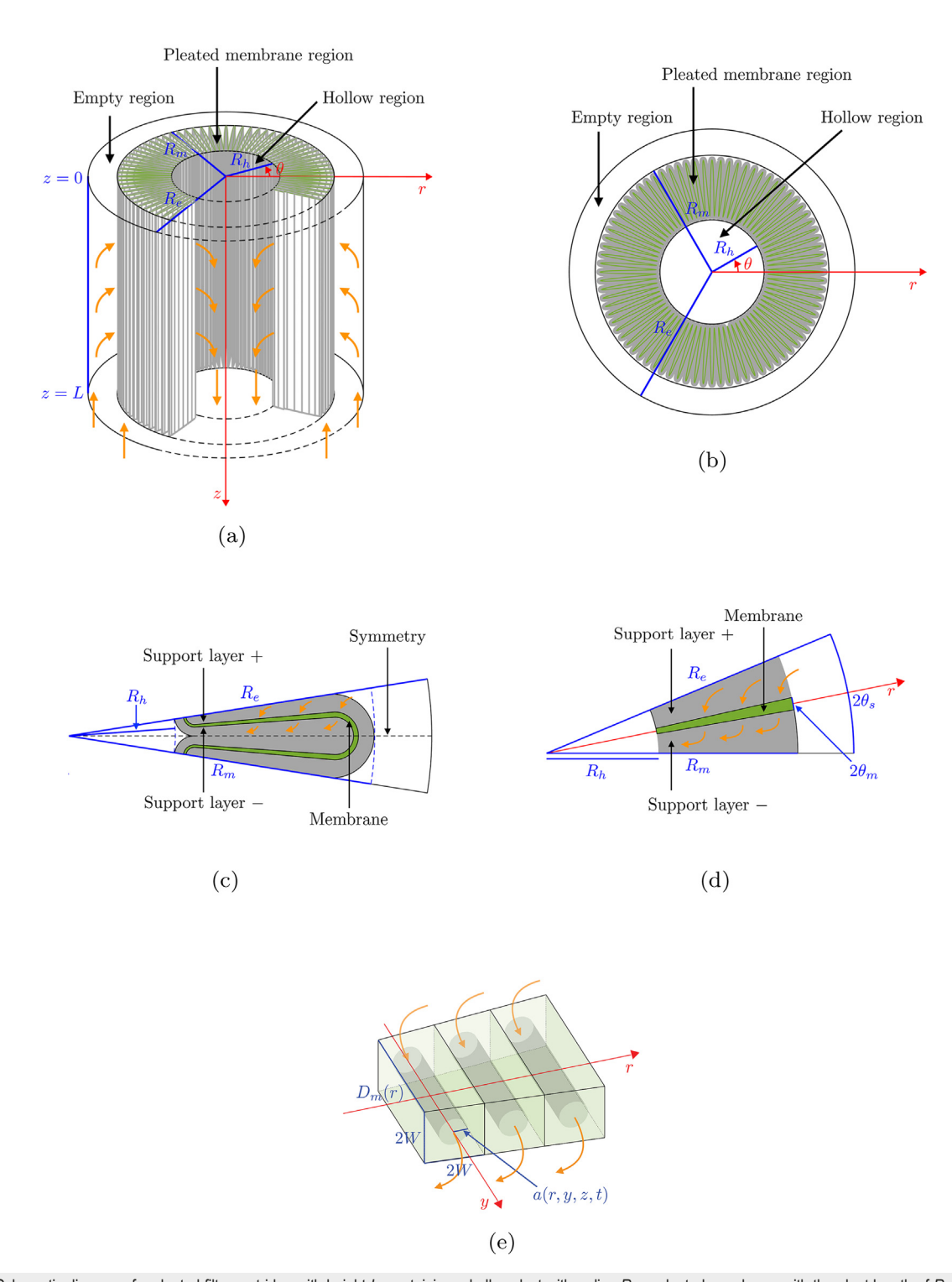


FIG. 1. (a) Schematic diagram of a pleated filter cartridge with height L, containing a hollow duct with radius R_h , a pleated membrane with the pleat length of $R_m - R_h$, and an empty region with radius R_e . Orange arrows indicate the flow direction. (b) Cross-sectional view of a pleated filter cartridge. The z-axis is perpendicular to the page. (c) Schematic of a single pleat, assumed to repeat periodically. Gray corresponds to support layers, and green represents the membrane (in reality much thinner than the support layers). Radial symmetry (black dashed line) is assumed about centerline of the pleat. Orange arrows indicate the flow direction. (d) Idealized geometry (half the pleat of a tightly packed pleated filter with support layers and membrane occupy the whole space without any air gaps) to be considered in our model with the same color coding as (c). Orange arrows indicate the flow direction. (e) Schematic diagram of the membrane pore structure with initial equal-sized radius a(r, y, z, t) contained within a trapezoidal prism of dimensions $2W \times 2W \times D_m(r)$, and the membrane consists of a periodic array of such trapezoidal prisms. Orange arrows indicate the flow direction.

from the hollow region, indicated by the orange arrows in Fig. 1. The outer and inner support layers are called, the support layers plus and minus as represented by + and -, with permeabilities k_{s+} and k_{s-} , respectively. Since the pores of both support layers are much larger than those of the membrane, the permeability of the support layers k_{s^i} (for $i \in \{+, -\}$) is assumed to be constant in both space and time t, which means no fouling occurs in these layers. The membrane is a thin filter sheet used to remove the undesired particles, which has thickness $D_m(r)$, length $R_m - R_h$, and height L along the y, r, and z axes, respectively, as shown collectively in Figs. 1(a), 1(d), and 1(e). In addition, we assume the typical membrane thickness is \tilde{D}_m . We consider the mass transport of the diluted particles with concentration c in the feed through the membrane. The fouling occurs within the membrane; therefore, its performance deteriorates in the course of time and as a result, the membrane permeability k_m evolves as a function of space and time. We assume the pleated membrane lies periodically between $y = -D_m(r)/2$ and $y = D_m(r)/2$. It is sandwiched between two support layers and pleated at angles of $2\theta_m$ and $2\theta_s$, which are the pleat angles for the membrane and support layers, respectively [see Fig. 1(d), which also shows $D_m(r) = 2r \sin \theta_m$]. Based on the pleated filter region geometry, we assume $\delta = \theta_m/\theta_s \ll 1$, and the membrane consists of pores with radius a(r, y, z, t) to be arranged in a series of trapezoidal prisms, which we approximate them with a series of repeating lattice of dimensions $2W \times 2W \times D_m(r)$ as shown in Fig. 1(e). Note that we neglect the curvature of the cartridge for the membrane. The membrane pores are assumed to be narrow and long and, hence, have a small aspect ratio, i.e., $\epsilon_p = W/D_m \ll 1$. This assumption implies that there are sufficiently a large number of pores in the membrane that they may be considered as continuously distributed with radius a(r, y, z, t). The flow and particle transport within the membrane pores are represented in an axisymmetric cylindrical coordinates (ρ, Φ, y) .

The typical thickness of the support layers is represented by D_s , which lies between the thickness (arc length) of the tip and valley of the support layers, i.e., $2\theta_sR_s < D_s < 2\theta_sR_m$. Then the number of pleats in the cylindrical filter is defined as $\mathcal{N} = \pi/\theta_s$. Note that θ_s is restricted such that \mathcal{N} is a positive integer. We also assume that the support layers are much thicker than the membrane layer but much smaller than the pleat length, i.e., $D_m \ll D_s \ll R_m - R_h$. We distinguish the support layers from the membrane layer by incorporating cylindrical coordinates with angular dependency, (r, θ, z) , while the membrane layer is described by the axisymmetric radial and axial directions with an additional direction indicating the depth through the membrane layer, i.e., (r, y, z) as shown in Fig. 1(e).

Since no fouling occurs in the empty region and the hollow region, we only consider the transport of particles due to a combination of diffusion, advection, and fouling within the pleated membrane. Adsorption of particle (fouling) occurs at different rates within the pleated membrane, depending on the local particle concentration and flow. The flow enters to the empty region of the filter cartridge along $R_m < r < R_e$ at z = L with constant inlet pressure P_0 and exits from the hollow region along $0 < r < R_h$ at z = L with constant outlet pressure 0. The pressure drop drives the fluid through the pleated region, and a particular quantity of interest is the total throughput through the filter cartridge and the amount of particle concentration in the filtrate, which will be explained in detail later.

III. GOVERNING EQUATIONS

We now outline the governing equations for each of the three regions of the pleated filter cartridge: the empty region, the pleated filter region (consists of a support layer plus region, a membrane, and a support layer minus region), and the hollow region.

A. Empty region

Since no fouling occurs in the empty region, we do not need to model the particle transport in this region; therefore, we only focus on the fluid flow. Additionally, since we consider pleated filter with high pleat packing density, the azimuthal dependence of the fluid velocity in the empty (as well as hollow) region is asymptotically small and may be neglected despite the azimuthal dependence of the geometry in the membrane region. The details of the asymptotic analysis based on small limit of θ_s are omitted here for brevity. Therefore, we describe the flow in the empty region by the incompressible axisymmetric Stokes equations in cylindrical coordinates (r, θ, z) , as

$$\nabla p_e = \mu \nabla^2 \mathbf{u}_e, \quad \nabla \cdot \mathbf{u}_e = 0,$$

in $R_m \le r \le R_e, \quad 0 \le z \le L,$ (1)

where μ is the dynamic viscosity of the fluid and p_e and u_e are the flow pressure and velocity in the empty region, respectively. Note that $u_e = (u_e, 0, w_e)$, where u_e and w_e denote the radial and axial velocities, respectively. The specified inlet pressure at the bottom of the empty region, no flux at the top of the cartridge, and no slip velocity at the cartridge housing wall are some of the boundary conditions for the pressure and velocity in the empty region, which are

$$p_e|_{z=L} = p_0, \quad u_e|_{z=0} = 0, \quad u_e|_{r=R_e} = 0,$$
 (2)

respectively. There are more boundary conditions for the empty region and the pleated region interface, which will be introduced later.

B. Pleated region

We model the flow through the pleated region by Darcy's law along with the continuity equation for the support layers in (r, θ, z) coordinates. Considering the flow pressure and velocity p_{s^i} and u_{s^i} (for $i \in \{+, -\}$) for the support layers, we have

$$\mathbf{u}_{s^i} = -\frac{k_{s^i}}{\mu} \nabla p_{s^i}, \quad \nabla \cdot \mathbf{u}_{s^i} = 0,$$

$$\mathbf{u}_{s^i} = (u_{s^i}, v_{s^i}, w_{s^i}), \quad i \in \{+, -\},$$
in $R_h \le r \le R_m, \quad \theta_m \le |\theta| \le \theta_s, \quad 0 \le z \le L.$ (3)

The boundary conditions for the empty region and pleated region interface are

$$\begin{aligned} p_{e}|_{r=R_{m}} &= p_{s^{+}}|_{r=R_{m}}, \quad u_{e}|_{r=R_{m}} = \phi u_{s^{+}}|_{r=R_{m}}, \\ \frac{\partial w_{e}}{\partial r}\Big|_{r=R_{m}} &= \frac{-\alpha}{\sqrt{k_{s^{+}}}} (w_{e} - w_{s^{+}})|_{r=R_{m}}, \end{aligned}$$
(4)

where ϕ is the local pleated membrane porosity³⁷ and is assumed to be constant. The last boundary condition represents a non-vanishing tangential slip velocity at the interface, ^{37–39} where α is a dimensionless slip constant that depends on the surface properties. Note that it is difficult to measure the slip coefficient α . This boundary condition

describes the physical flow phenomena in laminar flow fields above permeable blocks by the theoretical and experimental research. 40,41 The importance of the slip-boundary condition (4) is that it describes a slip velocity in the main flow direction at the interface between the porous support layers and the outer flow stream and is also consistent with flow phenomena. 39 In addition, the boundary conditions for the support layers follow as:

$$\frac{\partial p_{s^{+}}}{\partial r}\Big|_{r=R_{h}} = 0, \quad \frac{\partial p_{s^{+}}}{\partial \theta}\Big|_{\theta=\theta_{s}} = 0,
\frac{\partial p_{s^{+}}}{\partial z}\Big|_{z=0} = 0, \quad \frac{\partial p_{s^{+}}}{\partial z}\Big|_{z=L} = 0,
\frac{\partial p_{s^{-}}}{\partial r}\Big|_{r=R_{m}} = 0, \quad \frac{\partial p_{s^{-}}}{\partial \theta}\Big|_{\theta=-\theta_{s}} = 0,
\frac{\partial p_{s^{-}}}{\partial z}\Big|_{z=0} = 0, \quad \frac{\partial p_{s^{-}}}{\partial z}\Big|_{z=L} = 0,$$
(6)

where θ_s is the pleat angle at the support layer. These boundary conditions are related to the no flux conditions at the tips $(r=R_h)$ and valleys $(r=R_m)$ of the pleated region, the symmetry lines in the support layers (see Fig. 1), and the no flux condition at the top (z=0) and bottom (z=1) ends of the cartridge. The boundary conditions for the pleated region and the hollow region interface will be given later.

Due to the small aspect ratio of membrane pores, we consider the flow through the membrane to be unidirectional in the y direction along the membrane pores' depth [see Fig. 1(e)] with pressure and velocity p_m and u_m , respectively, and follows Darcy's law and continuity equation:²⁹

$$u_m(r,t) = -\frac{k_m}{\mu} \frac{\partial p_m}{\partial y}, \quad \frac{\partial u_m}{\partial y} = 0, \quad k_m = \frac{\pi a^4}{32W^2},$$
in $R_h \le r \le R_m, \quad -\frac{D_m(r)}{2} \le y \le \frac{D_m(r)}{2}, 0 \le z \le L,$ (7)

where k_m is the membrane permeability and is related to the local pore radius a by the Hagen–Poiseuille formula. ⁴² Note that the dimensional membrane permeability k_m has dimension length square. In addition, the continuity of flux between the support layers and membrane gives

$$u_{m} = -\frac{k_{s^{+}}}{\mu} \frac{1}{r} \frac{\partial p_{s^{+}}}{\partial \theta} \bigg|_{\theta = \frac{\theta_{m}}{2}} = -\frac{k_{s^{-}}}{\mu} \frac{1}{r} \frac{\partial p_{s^{-}}}{\partial \theta} \bigg|_{\theta = -\frac{\theta_{m}}{2}},$$
(8)
$$R_{h} \leq r \leq R_{m}, \quad 0 \leq z \leq L.$$

The flow within the membrane pores is assumed to be axisymmetric in the cylindrical coordinates (ρ, Φ, y) , and the flow velocity $u_p = (u_p, 0, w_p)$ links with the cross-sectionally averaged velocity of the fluid within the pore V_p and superficial Darcy velocity u_m by

$$V_p = \frac{1}{\pi a^2} \int_0^a \int_0^{2\pi} |\mathbf{u}_p| \, r \, d\theta \, dr, \quad 4W^2 u_m = \pi a^2 V_p \tag{9}$$

and satisfies the Stokes equations

$$\nabla p_p = \mu \nabla^2 \mathbf{u}_p, \quad \nabla \cdot \mathbf{u}_p = 0,$$
in $0 \le \rho \le a$, $R_h \le r \le R_m$,
$$-\frac{D_m(r)}{2} \le y \le \frac{D_m(r)}{2}, \quad 0 \le z \le L,$$
(10)

where p_p is the flow pressure within a pore. The boundary conditions for the pressure at the membrane and support layers interface as well as no slip velocity condition on the membrane pores walls are

$$p_{p}|_{y=\frac{D_{m}(r)}{2}} = p_{s^{+}}|_{\theta=\frac{\theta_{m}}{2}}, \quad p_{p}|_{y=-\frac{D_{m}(r)}{2}} = p_{s^{-}}|_{\theta=-\frac{\theta_{m}}{2}},$$

$$\mathbf{u}_{p} \cdot \mathbf{n}|_{\theta=a} = 0, \quad \mathbf{u}_{p} \cdot \mathbf{t}|_{\theta=a} = 0,$$
(11)

where $\mathbf{n} = \frac{\nabla(\rho - a)}{|\nabla(\rho - a)|}$ and \mathbf{t} are the unit normal and tangent vectors to the membrane pores walls, respectively.

In order to model the mass transport of the particles in the feed through the membrane pores, we consider an axisymmetric advection-diffusion equation in the cylindrical coordinates (ρ, φ, y) for the particle concentration c,

$$\frac{\partial c}{\partial t} + \nabla \cdot \mathbf{Q}_p = 0, \quad \mathbf{Q}_p = -\Xi \nabla c + \mathbf{u}_p c,
\text{in } 0 \le \rho \le a, \quad R_h \le r \le R_m,
-\frac{D_m(r)}{2} \le y \le \frac{D_m(r)}{2}, \quad 0 \le z \le L,$$
(12)

where \mathbf{Q}_p is the total particle flux and Ξ is the diffusion coefficient of particles in the feed solution. We assume the particle concentration is constant at the membrane inlet and continuity of particle concentration at the bottom and wall of the pore. Physically, the first boundary condition could correspond to our filter inlet (or membrane inlet since no fouling can occur in the empty region) being in contact with a very large reservoir containing a very small concentration of the particles. Imagine that the reservoir is so large that, even when some of the particles diffuse into the membrane, the concentration within the reservoir stays approximately constant. The detailed justification can be found in Ref. 3. Mathematically, the boundary conditions may be expressed as

$$c|_{y=\frac{D_m(r)}{2}} = C_0, \quad \frac{\partial c}{\partial y}\Big|_{y=-\frac{D_m(r)}{2}} = 0,$$

$$\mathbf{Q}_p \cdot \mathbf{n}|_{\rho=a} = -\Lambda c|_{\rho=a},$$
(13)

where C_0 and Λ are the particle concentration at the membrane pore inlet and the particle-wall attraction coefficient (or stickiness coefficient, describing particles deposition on the pores wall), respectively. Following earlier works, 3,43 the rate of local pore radius shrinkage is proposed to proportional to the local concentration of particles. Specifically, we assume the local pore cross-sectional area shrinks at a rate proportional to the particle-wall attraction coefficient Λ , the void fraction of particle locally (ηc , where η is an effective particle volume), and the local pore circumference available for particles to adhere to

$$\frac{\partial(\pi a^2)}{\partial t} = 2\pi a \frac{\partial a}{\partial t} = -\Lambda \eta c (2\pi a) \iff \frac{\partial a}{\partial t} = -\Lambda \eta c,$$
in $R_h \le r \le R_m$, $-\frac{D_m(r)}{2} \le y \le \frac{D_m(r)}{2}$, (14)
$$0 \le z \le L.$$

This equation simply says that the pore cross-sectional volume per unit depth shrinks at a rate given by the total volume of particles deposited locally. ^{6,44} The initial pore radius is prescribed, and we assume the membrane consists of identical cylindrical pores initially, i.e.,

$$a(r, y, z, t = 0) = a_0.$$
 (15)

C. Hollow region

Similar to the empty region, we utilize the Stokes equations in cylindrical coordinates (r,θ,z) without any angular dependency for the hollow region, i.e.,

$$\nabla p_h = \mu \nabla^2 \mathbf{u}_h, \quad \nabla \cdot \mathbf{u}_h = 0,$$

in $0 \le r \le R_h, \quad 0 \le z \le L,$ (16)

where p_h and u_h are the flow pressure and velocity in the hollow region, respectively. Note that $u_h = (u_h, 0, w_h)$, where u_h and w_h denote the radial and axial velocities, respectively. The boundary conditions for the pleated region and the hollow region interface are

$$p_{s^{-}}|_{r=R_{h}} = p_{h}|_{r=R_{h}}, \quad \phi u_{s^{-}}|_{r=R_{h}} = u_{h}|_{r=R_{h}},$$

$$\frac{\partial w_{h}}{\partial r}\Big|_{r=R_{h}} = \frac{-\alpha}{\sqrt{k_{s^{-}}}} (w_{h} - w_{s^{-}})|_{r=R_{h}},$$
(17)

and the boundary conditions for the hollow region follow:

$$p_h|_{z=L} = 0, \quad \mathbf{u}_h|_{z=0} = \mathbf{0}, \quad u_h|_{r=0} = \frac{\partial w_h}{\partial r}\Big|_{r=0} = 0.$$
 (18)

IV. NONDIMENSIONALIZATION

To reduce the number of independent parameters, we use the following scalings to nondimensionalize the model (1)–(18) for the empty region, pleated and hollow regions given in Secs. III A–III C, respectively,

$$p_{i} = P_{0}\hat{p}_{i}, \quad i \in \{e, s^{+}, m, s^{-}, h\},$$

$$(r, \theta, z) = L\left(\epsilon_{m}\hat{r}, \frac{\theta_{s}}{L}\hat{\theta}, \hat{z}\right),$$

$$(u_{i}, w_{i}) = \frac{\epsilon_{m}^{2}LP_{0}}{\mu}(\epsilon_{m}\hat{u}_{i}, \hat{w}_{i}), \quad i \in \{e, h\},$$

$$(u_{s^{i}}, v_{s^{i}}, w_{s^{i}}) = \frac{KP_{0}}{\mu R_{m}}(\hat{u}_{s^{i}}, \hat{v}_{s^{i}}, \epsilon_{m}\hat{w}_{s^{i}}), \quad i \in \{+, -\},$$

$$(\rho, y, D_{m}(r)) = \tilde{D}_{m}(\epsilon_{p}\hat{\rho}, \hat{y}, \hat{D}_{m}(\hat{r})),$$

$$(a, a_{0}) = W(\hat{a}, \hat{a}_{0}), \quad c = C_{0}\hat{c}, \quad t = \frac{W}{\Lambda\eta C_{0}}\hat{t}, \qquad (19)$$

$$(u_{p}, w_{p}, u_{m}, V_{p}) = \frac{\pi P_{0}W^{2}}{32\mu \tilde{D}_{m}}(\epsilon_{p}\hat{u}_{p}, \hat{w}_{p}, \hat{u}_{m}, \hat{V}_{p}),$$

$$\phi = \phi_{0}\hat{\phi}, \quad \phi_{0} = \frac{L^{2}\epsilon_{m}^{4}}{K} \quad k_{s^{+}} = k_{s^{-}} = k = K\hat{k},$$

$$k_{m} = \frac{\pi W^{2}}{32}\hat{k}_{m}, \quad \text{Pe} = \frac{\pi P_{0}W^{2}}{32\Xi\mu} \quad \alpha_{0} = \frac{\epsilon_{m}^{2}L\alpha}{\sqrt{K}},$$

$$\Gamma = \frac{\pi R_{m}W^{2}}{32K\theta_{s}\tilde{D}_{m}}, \quad \lambda = \frac{64\mu\Lambda\tilde{D}_{m}^{2}}{\pi P_{0}W^{3}},$$

where hats demonstrate the dimensionless variables. We assume the permeability of the support layers is equal, i.e., $k_{s^+} = k_{s^-} = k$. Here, K is the average support layer permeability in the radial direction, Pe is the Péclet number, defined as the ratio of advective transport rate to that of diffusive, Γ is the scaled measure of the relative importance of

the resistance of the packing material to that of the membrane, 30,32 and λ is the dimensionless particle–wall attraction coefficient. According to Tables I and II, we assume

$$\epsilon_{m} = \frac{R_{m}}{L} \ll 1, \quad l = \frac{R_{h}}{R_{m}}, \quad d = \frac{R_{e} - R_{m}}{R_{m}},$$

$$\epsilon_{p} = \frac{W}{\tilde{D}_{m}} \ll 1, \quad \delta = \frac{\theta_{m}}{\theta_{s}} \ll 1,$$

$$\phi_{0} = \mathcal{O}(1), \quad \text{Pe} = \mathcal{O}(1), \quad \alpha_{0} \geq \mathcal{O}(\epsilon_{m}).$$
(20)

In addition, for simplifying the equations, we assume $\tilde{D}_m \approx 2R_m \sin \theta_m$ as a consequence of $\hat{D}_m(\hat{r}) \approx \hat{r}$.

A. Empty region

We use scalings (19) in (1) and (2) and then drop hats to obtain the dimensionless model for the empty region as

$$\frac{\partial p_e}{\partial r} = \epsilon_m^2 \frac{1}{r} \frac{\partial}{\partial r} \left(r \frac{\partial u_e}{\partial r} \right) + \epsilon_m^4 \frac{\partial^2 u_e}{\partial z^2} - \epsilon_m^2 \frac{u_e}{r^2},
\frac{\partial p_e}{\partial z} = \frac{1}{r} \frac{\partial}{\partial r} \left(r \frac{\partial w_e}{\partial r} \right) + \epsilon_m^2 \frac{\partial^2 w_e}{\partial z^2},
\frac{1}{r} \frac{\partial}{\partial r} (r u_e) + \frac{\partial w_e}{\partial z} = 0,
\text{in } 1 \le r \le 1 + d, \quad 0 \le z \le 1$$
(21)

with the boundary conditions

$$p_e|_{z=1} = 1, \quad u_e|_{z=0} = w_e|_{z=0} = 0,$$

 $u_e|_{r=1+d} = w_e|_{r=1+d} = 0.$ (22)

B. Pleated region

Similarly, we nondimensionalize (3)–(15) by using the scalings given in (19) to obtain

TABLE I. Dimensional parameter values. 29,32,33,46-48

Parameter	Description	Typical value
L	Length of the pleats	0.2 - 0.5 m
R_e	Radius of the empty region	3 - 4.5 cm
R_h	Radius of the hollow region	1 - 1.5 cm
R_m	Radius of the membrane region	2 - 3 cm
D_s	Support layer thickness	1 mm
D_m	Membrane thickness	$300 \mu \mathrm{m}$
θ_s	Support layers pleat angle	$\pi/5 - \pi/540$
θ_m	Membrane pleat angle	$\pi/50 - \pi/5400$
P_0	Pressure drop	10 – 100 kPa
K	Average support layer permeability	10^{-11} m^2
2 W	Width of repeating lattice	$4.5~\mu\mathrm{m}$
μ	Viscosity of feed	0.001 Pa s
Λ	Particle-wall attraction coefficient	Unknown
Ξ	Diffusion coefficient	$10^{-11} - 10^{-5} \text{ m}^2 \text{s}^{-1}$

TABLE II. Dimensionless parameter values. 29,32,33,46-48

Parameter	Formula/Description	Typical value
ϵ_m	R_m/L	0.04 - 0.15
d	$(R_e - R_m)/R_m$	0.03 - 1.25
l	R_h/R_m	0.5
Δ	θ_m/θ_s	0.1
ϵ_p	W/D_m	0.0075
$\dot{\phi}$	Pleated membrane porosity	0.01 - 0.9
Pe	$(\pi P_0 W^2)/(32\Xi \mu)$	$1 - 10^6$
A	Slip constant	0.01 - 1
α_0	$\epsilon_m^2 L\alpha/\sqrt{K}$	1 - 100
Λ	$(64\mu\Lambda D_m^2)/(\pi P_0 W^3)$	Unknown; value 2 used
\mathcal{N}	$\pi/ heta_s$	5 - 540
Γ	$(\pi R_m W^2)/(32K\theta_s D_m)$	0.01 - 100
k	$(180\theta_s)/\pi$	0.33 - 36

$$u_{s^{i}} = -k \frac{\partial p_{s^{i}}}{\partial r}, \quad v_{s^{i}} = -\frac{1}{\theta_{s}} \frac{k}{r} \frac{\partial p_{s^{i}}}{\partial \theta}, \quad w_{s^{i}} = -k \frac{\partial p_{s^{i}}}{\partial z},$$

$$\frac{1}{r} \frac{\partial}{\partial r} \left(rk \frac{\partial p_{s^{i}}}{\partial r} \right) + \frac{k}{r^{2}} \frac{1}{\theta_{s}^{2}} \frac{\partial^{2} p_{s^{i}}}{\partial \theta^{2}} + \epsilon_{m}^{2} k \frac{\partial^{2} p_{s^{i}}}{\partial z^{2}} = 0,$$

$$i \in \{+, -\}, \quad \text{in} \quad l \leq r \leq 1, \quad \delta \leq |\theta| \leq 1, \quad 0 \leq z \leq 1,$$

$$(23)$$

with the boundary conditions for the empty region and pleated region interface

$$\begin{aligned} p_{e}|_{r=1} &= p_{s^{+}}|_{r=1}, \quad u_{e}|_{r=1} &= \phi u_{s^{+}}|_{r=1}, \\ \frac{\partial w_{e}}{\partial r}\Big|_{r=1} &= -\frac{\alpha_{0}}{\epsilon_{m}\sqrt{k}} \left(w_{e} - \frac{\epsilon_{m}}{\phi_{0}} w_{s^{+}}\right) \Big|_{r=1}, \end{aligned}$$
(24)

and the boundary conditions for the support layers

$$\frac{\partial p_{s^{+}}}{\partial r}\Big|_{r=l} = 0, \quad \frac{\partial p_{s^{+}}}{\partial \theta}\Big|_{\theta=1} = 0,
\frac{\partial p_{s^{+}}}{\partial z}\Big|_{z=0} = 0, \quad \frac{\partial p_{s^{+}}}{\partial z}\Big|_{z=1} = 0,
\frac{\partial p_{s^{-}}}{\partial r}\Big|_{r=1} = 0, \quad \frac{\partial p_{s^{-}}}{\partial \theta}\Big|_{\theta=-1} = 0,
\frac{\partial p_{s^{-}}}{\partial z}\Big|_{z=0} = 0, \quad \frac{\partial p_{s^{-}}}{\partial z}\Big|_{z=1} = 0.$$
(25)

The dimensionless Darcy's law, continuity, and membrane permeability (7) become

$$u_{m} = \frac{p_{s^{-}|\theta = -\frac{\delta}{2}} - p_{s^{+}|\theta = \frac{\delta}{2}}}{\int_{-\frac{\tau}{2}}^{\frac{\tau}{2}} \frac{dy}{a^{4}(y)}}, \quad k_{m} = a^{4},$$

$$\text{in } l \leq r \leq 1, \quad 0 \leq z \leq 1,$$

$$(27)$$

and the continuity of flux between the support layers, membrane and membrane pores, Eqs. (8) and (9), respectively, give the dimensionless membrane Darcy's velocity u_m , and the cross-sectionally averaged fluid velocity within the pores V_ρ as

$$u_{m} = -\frac{1}{\theta_{s}^{2} \Gamma} \frac{k}{r} \frac{\partial p_{s^{+}}}{\partial \theta} \bigg|_{\theta = \frac{\delta}{2}} = -\frac{1}{\theta_{s}^{2} \Gamma} \frac{k}{r} \frac{\partial p_{s^{-}}}{\partial \theta} \bigg|_{\theta = -\frac{\delta}{2}}, \tag{28}$$

$$V_p = \frac{1}{\pi a^2} \int_0^{2\pi} \int_0^a \sqrt{\epsilon_p^2 u_p^2 + w_p^2} \, r \, dr \, d\theta, \quad 4u_m = \pi a^2 V_p. \tag{29}$$

The dimensionless Stokes flow within the membrane pores and the associated boundary conditions are obtained from (10) and (11) as

$$\frac{\partial p_p}{\partial \rho} = \epsilon_p^2 \frac{1}{\rho} \frac{\partial}{\partial \rho} \left(\rho \frac{\partial u_p}{\partial \rho} \right) + \epsilon_p^4 \frac{\partial^2 u_e}{\partial y^2} - \epsilon_p^2 \frac{u_p}{\rho^2},$$

$$\frac{\partial p_p}{\partial y} = \frac{1}{\rho} \frac{\partial}{\partial \rho} \left(\rho \frac{\partial w_p}{\partial \rho} \right) + \epsilon_p^2 \frac{\partial^2 w_p}{\partial y^2},$$

$$\frac{1}{\rho} \frac{\partial}{\partial \rho} (\rho u_p) + \frac{\partial w_p}{\partial y} = 0,$$
in $0 \le \rho \le a, \quad l \le r \le 1,$

$$-\frac{r}{2} \le y \le \frac{r}{2}, \quad 0 \le z \le 1,$$

$$\left(-u_p + \epsilon_p \frac{\partial a}{\partial y} v_p \right) \Big|_{\alpha = \sigma} = 0 \quad \left(\epsilon_p \frac{\partial a}{\partial y} u_p + v_p \right) \Big|_{\alpha = \sigma} = 0. \quad (31)$$

We consider a quasi-static assumption, which stems from the fact that the membrane pores evolve on a much longer timescale compared to that of the transport of the fluid flow through the membrane pores. With this assumption, the particle transport (12) simplifies to

$$\frac{1}{\epsilon_p^2 \operatorname{Pe}} \left(\frac{1}{\rho} \frac{\partial}{\partial \rho} \left(\frac{\partial c}{\partial \rho} \right) + \epsilon_p^2 \frac{\partial^2 c}{\partial y^2} \right) = u_p \frac{\partial c}{\partial \rho} + w_p \frac{\partial c}{\partial y},$$
in $0 \le \rho \le a, \quad l \le r \le 1,$

$$-\frac{r}{2} \le y \le \frac{r}{2}, \quad 0 \le z \le 1,$$
(32)

with boundary conditions

$$c|_{y=\frac{r}{2}} = 1, \quad \frac{\partial c}{\partial y}\Big|_{y=-\frac{r}{2}} = 0,$$

$$\frac{1}{\epsilon_p^2 \operatorname{Pe}} \frac{\partial c}{\partial \rho} - \frac{1}{\operatorname{Pe}} \frac{\partial c}{\partial y} \frac{\partial a}{\partial y}\Big|_{\rho=a} = -\lambda c|_{\rho=a}.$$
(33)

Furthermore, (14) and (15) give the dimensionless pore radii shrinkage

$$\frac{\partial a}{\partial t} = -c,$$
in $0 \le \rho \le a, \quad l \le r \le 1,$

$$-\frac{r}{2} \le y \le \frac{r}{2}, \quad 0 \le z \le 1,$$
(34)

and the initial pore radii

$$a(r, y, z, t = 0) = a_0,$$
 (35)

respectively.

C. Hollow region

Finally, the dimensional equations (16)–(18) for the hollow region model given in Sec. III C are nondimensionalized as

$$\frac{\partial p_{h}}{\partial r} = \epsilon_{m}^{2} \frac{1}{r} \frac{\partial}{\partial r} \left(r \frac{\partial u_{h}}{\partial r} \right) + \epsilon_{m}^{4} \frac{\partial^{2} u_{h}}{\partial z^{2}} - \epsilon_{m}^{2} \frac{u_{h}}{r^{2}},$$

$$\frac{\partial p_{h}}{\partial z} = \frac{1}{r} \frac{\partial}{\partial r} \left(r \frac{\partial w_{h}}{\partial r} \right) + \epsilon_{m}^{2} \frac{\partial^{2} w_{h}}{\partial z^{2}},$$

$$\frac{1}{r} \frac{\partial}{\partial r} (r u_{h}) + \frac{\partial w_{h}}{\partial z} = 0,$$
(36)

with the boundary conditions for the pleated and the hollow regions' interface

$$p_{s^{-}}|_{r=l} = p_{h}|_{r=l}, \quad \phi u_{s^{-}}|_{r=l} = u_{h}|_{r=l},$$

$$\frac{\partial w_{h}}{\partial r}\Big|_{r=l} = -\frac{\alpha_{0}}{\epsilon_{m}\sqrt{k}} \left(w_{h} - \frac{\epsilon_{m}}{\phi_{0}} w_{s^{-}}\right)\Big|_{r=l},$$
(37)

and the boundary conditions for the hollow region

$$p_h|_{z=1} = 0, \quad u_h|_{z=0} = w_h|_{z=0} = 0,$$

$$u_h|_{r=0} = \frac{\partial w_h}{\partial r}\Big|_{r=0} = 0.$$
(38)

V. ASYMPTOTIC ANALYSIS

We perform an asymptotic analysis for the empty region and the hollow region by introducing a perturbation expansion of dependent variables in power of the slenderness parameter $\epsilon_m \ll 1$

$$x = x_0 + \epsilon_m x_1 + \epsilon_m^2 x_2 + \cdots, \quad x \in \{u_e, u_h, p_e, p_h\}.$$
 (39)

Additionally, for the support layers and membrane pores, we utilize

$$x = x_0 + \theta_s^2 x_1 + \theta_s^4 x_2 + \cdots, \quad x \in \{ \mathbf{u}_{s^i}, p_{s^i} \}, \quad i \in \{+, -\} \quad (40)$$

and

$$x = x_0 + \epsilon_p x_1 + \epsilon_p^2 x_2 + \cdots, \quad x \in \{u_p, p_p, c\},$$
 (41)

respectively, where $\theta_s \ll 1$ and $\epsilon_p \ll 1$.

A. Empty region

Substituting the expansion (39) into the first part of (21) gives that the pressure is independent of r to leading order in ϵ_m , i.e., $p_{e_0} = p_{e_0}(z)$. With this, the second part of (21) and the boundary conditions for the axial velocity in the empty region given in the third part of (22), along with the leading order of the third boundary condition in (24) (which is $w_{e_0}|_{r=1} = 0$), we obtain

$$w_{e_0} = \frac{1}{4} \frac{dp_{e_0}}{dz} (r^2 - 1 + \gamma \ln r), \quad \gamma = \frac{1 - (1 + d)^2}{\ln (1 + d)}.$$
 (42)

Then (42) along with the third part of (21) and the rest of boundary conditions in (22) give

$$u_{e_0} = -\frac{1}{16}M(r)\frac{d^2p_{e_0}}{dz^2},$$

$$M(r) = r(r^2 - 2 + \gamma(2\ln r - 1))$$

$$-\frac{(1+d)^2}{r}[(1+d)^2 - 2 + \gamma(2\ln(1+d) - 1)].$$
(43)

B. Pleated region

Using the expansion (40) for the support layer plus region into the second part of (23) gives that the pressure is independent of θ_s , i.e., $p_{s_0^+}(r,z)$. We apply $\int_{\delta/2}^1 d\theta$ to $\mathcal{O}(\theta_s^2)$ of the second part of (23) along with the second condition in (25) to obtain

$$\left(1 - \frac{\delta}{2}\right) \frac{\partial}{\partial r} \left(rk \frac{\partial p_{s_0^+}}{\partial r}\right) = \frac{k}{r} \frac{\partial p_{s_1^+}}{\partial \theta}\Big|_{\theta = \frac{\delta}{2}}.$$
 (44)

We then use the leading order of (27) and (28) in (44) to arrive at

$$\left(1 - \frac{\delta}{2}\right) \frac{\partial}{\partial r} \left(rk \frac{\partial p_{s_0^+}}{\partial r}\right) = \frac{\Gamma}{\int_{-r/2}^{r/2} \frac{dy}{a^4(y)}} (p_{s_0^+} - p_{s_0^-})$$

$$= -\Gamma u_{m_0}. \tag{45}$$

In addition, by plugging the leading order of the first part of (23) and the middle boundary condition of (24) into (43), we arrive at

$$k \frac{\partial p_{s_0^+}}{\partial r} \bigg|_{r=1} = \frac{M(1)}{16\phi} \frac{d^2 p_{e_0}}{dz^2}.$$
 (46)

Similarly, for the support layer minus region, we obtain

$$-\left(1 - \frac{\delta}{2}\right) \frac{\partial}{\partial r} \left(rk \frac{\partial p_{s_0^-}}{\partial r}\right) = \frac{\Gamma}{\int_{-r/2}^{r/2} \frac{dy}{a^4(y)}} (p_{s_0^+} - p_{s_0^-})$$

$$= -\Gamma u_{m_0}. \tag{47}$$

Note that, at the leading order, the cross-sectionally averaged velocity of the fluid within the pore and Darcy velocity (29) simplifies

$$V_{p_0} = \frac{1}{\pi a^2} \int_0^a \int_0^{2\pi} w_{p_0} r \, d\theta \, dr, \quad 4u_{m_0} = \pi a^2 V_{p_0}. \tag{48}$$

For the membrane layer, substituting the expansion (41) into the first part of (30) gives that the pressure is independent of ρ to the leading order in ϵ_p , i.e., $p_{p_0} = p_{p_0}(y)$. With this, the rest of (30) and the boundary conditions given in (31), we obtain

$$w_{p_0} = \frac{8}{\pi} (\rho^2 - a^2) \frac{\partial p_{p_0}}{\partial y},$$

$$u_{p_0} = \frac{2}{\pi} \frac{\partial}{\partial y} \left((\rho^3 - 2a^2 \rho) \frac{\partial p_{p_0}}{\partial y} \right),$$

$$p_{p_0} = p_{s_0^+} + (p_{s_0^-} - p_{s_0^+}) \frac{\int_{y}^{r/2} \frac{dy'}{a^4}}{\int_{-r/2}^{r/2} \frac{dy'}{a^4}}.$$
(49)

Similarly, after some manipulation,³⁶ the particle concentration transport (32) and (33) simplify to

$$-\frac{1}{\text{Pe}}\frac{\partial^2 c_0}{\partial y^2} + \left(V_{p_0} - \frac{2}{\text{Pe}}\frac{1}{a}\frac{\partial a}{\partial y}\right)\frac{\partial c_0}{\partial y} + \frac{\lambda}{a}c_0 = 0 \tag{50}$$

to the leading order in ϵ_p , with boundary conditions

$$c_0|_{y=\frac{r}{2}} = 1, \quad \frac{\partial c_0}{\partial y}|_{y=-\frac{r}{2}} = 0.$$
 (51)

Finally, (34) and (35) become

$$\frac{\partial a}{\partial t} = -c_0, \quad a(y, r, \theta, z, t = 0) = a_0. \tag{52}$$

Note that reduction of (32) to (50) is valid not only for $Pe = \mathcal{O}(1)$ but also for all Pe $< \mathcal{O}(1/\epsilon_p^2)$.

C. Hollow region

Similar to what we did in Sec. VA, in the leading order, (36)-(38) simplify to

$$w_{h_0} = \frac{1}{4} \frac{dp_{h_0}}{dz} (r^2 - l^2), \tag{53}$$

$$u_{h_0} = -\frac{1}{16} \frac{d^2 p_{h_0}}{dz^2} r(r^2 - 2l^2), \tag{54}$$

$$-k \frac{\partial p_{s_0^-}}{\partial r}\bigg|_{r=l} = \frac{l^3}{16\phi} \frac{d^2 p_{h_0}}{dz^2}.$$
 (55)

VI. SUMMARY AND NUMERICAL METHOD

By subtracting (45) and (47) and then integrating over r two times, we find a relation between the leading order pressures in the support layers, $p_{s_0^+}$ and $p_{s_0^-}$

$$p_{s_0^-} = -p_{s_0^+} + B_8 \int_I^r \frac{dr'}{r'k(r')} + B_9, \tag{56}$$

where $B_8(z)$ and $B_9(z)$. The leading orders of the first parts of both boundary conditions in (25) and (26) along with (46), (55), and (56) give the equation for $B_8(z)$ as

$$B_8 = \frac{M(1)}{16\phi} \frac{d^2 p_{e_0}}{dz^2} = -\frac{l^4}{16\phi} \frac{d^2 p_{h_0}}{dz^2}.$$
 (57)

The boundary conditions for (57) can be obtained from the leading orders of the first and second parts of both (22) and (38) as

$$\begin{aligned} p_{e_0}|_{z=1} &= 1, \quad \frac{\partial p_{e_0}}{\partial z}\Big|_{z=0} &= 0, \\ p_{h_0}|_{z=1} &= 0, \quad \frac{\partial p_{h_0}}{\partial z}\Big|_{z=0} &= 0, \end{aligned}$$

$$(58)$$

where the second parts of both (22) and (38) are related to no flux condition at the top of cartridge. Solving (57) and (58) gives

$$p_{e_0} = \frac{16\phi}{M(1)} (F(z) - F(1)) + 1,$$

$$p_{h_0} = -\frac{16\phi}{4} (F(z) - F(1)),$$
(59)

where

$$F(z) = \int_0^z \int_0^{z'} B_8(z'') dz'' dz', \quad F(0) = F'(0) = 0.$$
 (60)

In addition, we use (56) in (45) to obtain a boundary value problem for $p_{s_0^+}$ as

$$\left(1 - \frac{\delta}{2}\right) \frac{\partial}{\partial r} \left(rk \frac{\partial p_{s_0^+}}{\partial r}\right) - \frac{2\Gamma}{\int_{-r/2}^{r/2} \frac{dy}{a^4(y)}} p_{s_0^+} + \frac{\Gamma}{\int_{-r/2}^{r/2} \frac{dy}{a^4(y)}} \left(B_8 \int_l^r \frac{dr'}{r'k(r')} + B_9\right) = 0.$$
(61)

The boundary conditions for (61) can be obtained from the first parts of the boundary conditions in (24)-(26) and (37) along with (56) and (58) as

$$\begin{split} \frac{\partial p_{s_0^+}}{\partial r}\bigg|_{r=l} &= 0, \quad p_{s_0^+}|_{r=1} = \frac{16\phi}{M(1)}(F(z) - F(1)) + 1, \\ p_{s_0^+}|_{r=l} &= \frac{16\phi}{l^4}(F(z) - F(1)) + B_9, \quad \frac{\partial p_{s_0^+}}{\partial r}\bigg|_{r=1} = \frac{B_8}{k(1)}. \end{split} \tag{62}$$

Our model consists of various dimensional and dimensionless parameters shown in Tables I and II, respectively, with typical ranges of values in practice. Although a high level of variability or uncertainty in some parameter values such as Λ is noted in Table I, in practice users and filter membrane manufacturers should together be able to provide values or estimates for the particle wall attraction coefficient Λ listed in Table I for specific applications. In practice, it is difficult to estimate Λ and will require preliminary experiments. Methods, such as fluorescence microscopy, 49 with particles in the feed suspension fluorescently tagged, can be used to estimate Λ by comparing solutions of Eq. (14) to experimental images that reveal the density and location of particles trapped within the filter. Given the number of parameters, many will be held fixed in this investigation. Our numerical scheme is based on second-order accurate finite difference spatial discretization of (50), (51), and (60)–(62) in y, z, and r accordingly with a simple first-order implicit time step in the pore radius shrinkage equation (52), and trapezoidal quadrature to find the integrals in (56), (60), and (61). The solution scheme for this system is straightforward:

- 1. For given d, l, δ , ϕ , Pe, Γ , λ , k(r, z) and assigned $a(r, y, z, 0) = a_0$ at t = 0, solve (60)–(62) to obtain $p_{s_0^+}$, B_8 , and B_9 .
- 2. Use these resulting values into (56) to find $p_{s_0^-}$. $p_{s_0^+}$, $p_{s_0^-}$ and (47) gives u_{m_0} and then find V_{p_0} from (48). 3. Use V_{p_0} to solve (50) and (51) for c_0 .
- 4. Update the membrane pore radii in (52).
- 5. Return to step (1) and repeat until the membrane pore radii $a \rightarrow 0$.

VII. RESULTS

In this section, we present and analyze simulation of the models summarized in Sec. VI, focusing on how filtration performance depends on the key parameters governing the particle transport and pleat packing density. The Péclet number Pe measures the ratio of advective to axial-pore diffusive transport. At low Pe numbers, axialpore diffusion becomes appreciable. On the other hand, at larger Pe numbers, purely advection phenomena should become more prominent. Our model contains three dimensionless parameters that affect the pleat packing density (see Table II): \mathcal{N} , the number of pleats in the filter cartridge; Γ , measures the relative importance of the resistance of the packing material (the supporting material) to that of the

membrane; and k, the support layer permeability function is assumed constant but depends on how tightly compressed the pleats are. Higher pleat packing density indicates the supporting material provides most of the overall system resistance, whereas if the pleat packing density is lower the membrane contributes most of the overall system resistance. 29,32

There are several quantities that can be used to evaluate membrane performance. First, we define the average membrane porosity $\varphi(z,t)$, which is averaged across the pore length [-1/2,1/2] and the radial direction of the membrane $(l \le r \le 1)$,

$$\varphi(z,t) = \frac{\pi}{4} \int_{1}^{1} \int_{-1/2}^{1/2} a^{2}(r,y,z,t) \, dy \, dr. \tag{63}$$

The total dimensionless volumetric flux Q(t) through the pleated membrane filter is given by

$$Q(t) = \int_{0}^{1} \int_{1}^{1} V_{p_0}(r, z, t) dr dz, \tag{64}$$

and the volumetric throughput V(t), represents the total cumulative volume of filtrate processed by time t, is defined as the time integral of the volumetric flux Q(t),

$$\mathcal{V}(t) = \int_0^t \mathcal{Q}(t') \, dt'. \tag{65}$$

Another important performance metric is the averaged particle concentration at the downstream side of the membrane y = -1/2, $c_{avg}(t)$ is defined as

$$c_{avg}(t) = \frac{\int_{0}^{1} \int_{l}^{1} V_{p_0} c\left(r, -\frac{1}{2}, z, t\right) dr dz}{\mathcal{Q}(t)}.$$
 (66)

Note that this represents the averaged particle concentration in the filtrate at any given time.

To examine the effect of advection and axial-pore diffusion on the filtration efficiency, we vary the Péclet number $Pe = (\pi P_0 W^2)/$ $(32\Xi\mu)$, here assumed to vary due to changes in the dimensional diffusion coefficient \(\mathbb{\Xi}\). Figure 2 illustrates pore radius evolution as a function of dimensionless pore length y, at various times during the filtration process at two different (r, z) locations in the pleated membrane region, for two values of Péclet number with parameter values as given in the figures' captions. Note that, we assume $Pe = (\pi P_0 W^2)/2$ $(32\Xi\mu)$ is constant throughout each simulation; however, as time passes and the filter performance deteriorates via a combination of fouling mechanisms, the particle diffusion becomes significant. In other words, in a slow filtration process or during the late stages of filtration when the flow rate is naturally very low due to high level of fouling, particle diffusion plays a more important role. At this point, assuming Pe = 1 is physical and logical. For the case when axial-pore diffusion is comparable to advection (Pe = 1), we observe that the pore radius shrinks in time throughout the pore due to fouling with the most rapid pore shrinkage at the upstream of the pore, y = 0.5, for both selected locations: top-center of the pleated membrane, (r, z) = (0.75, 0) [Fig. 2(a)] and bottom-center of the pleated membrane, (r, z) = (0.75, 1)[Fig. 2(b)]. Since the rate of particle transport is increased due to the presence of axial-pore diffusion effect [see Eq. (50)] which enables more fouling further downstream of the pore. For the case where particle transport is dominated by advection (Pe $\rightarrow \infty$), the pore shrinkage at the upstream of the pore, y = 0.5, is much more rapid while the downstream portions of the pore remain minimally [Fig. 2(c)] to moderately [Fig. 2(d)] used for particle removal, reflecting the fact that the pores foul primarily at the upstream side due to the dominant mode of particle transport changes from the faster advection-diffusion to the slower advection-dominated [see Eq. (50)]. This is especially true for pores located at the top of the membrane filter, (r, z) = (0.75, 0), as demonstrated in Fig. 2(c). In both cases, we note that there is nearly no r variation in the evolution of pore radius in the pleated membrane region. Thus, we presented only selected results (center of membrane, r = 0.75) to illustrate different types of pore evolution our model can exhibit. Therefore, we can conclude that for designing the pleated membranes operating under high Péclet numbers, the filter membrane pores should be wider at the upstream side in order to use most of the membrane for the particle separation.^{4,30}

To gain insight into the evolution of the porosity of the membrane due to the effect of particle transport, in Fig. 3, we graph the average porosity $\varphi(z,t)$ [see the definition in (63)] as a function of dimensionless filter height z at various times throughout the evolution for two different values of Pe with parameter values as given in the figure caption. Figure 3(a) reveals that, when axial diffusion and advection are comparable (Pe = 1), $\varphi(z,t)$ decreases in time and remains relatively uniform along the filter height z over the entire duration of the simulation with only slightly lower value near the bottom of the filter, z=1. The results here are consistent with those presented in Figs. 2(a) and 2(b); in particular, the presence of axial-pore diffusion enables a more uniform fouling in the filter-axial direction. When the particle transport becomes advection-dominated (Pe $\rightarrow \infty$), however, we see that $\varphi(z,t)$ decreases in time at a much slower rate [see Fig. 3(b)]. We also observe that $\varphi(z,t)$ remains nearly uniform near the top of the filter, z=0 and monotonically decreases with the filter height z. Again, the effect of axial-pore diffusion increases the rate of particle transport, which enables more fouling to occur further downstream of the pore, resulting in overall lower average porosity throughout the filter.

Two common important characterizations of filter membrane performance are to plot the total instantaneous flux of filtrate through the membrane [see (64)] and the averaged particle concentration remain in the filtrate [see (66)] against the cumulative filtrate throughput at that time [see (65)]. Figures 4(a) and 4(b) show the dimensionless flux Q(t), and instantaneous particle concentration in the filtrate $c_{avg}(t)$ as functions of the dimensionless throughput V(t), respectively, as the Péclet number Pe varies from 1 (particle transport by advection and axial diffusion) to ∞ (particle transport by advection only) with parameter values as given in the figure caption. Note that $\mathcal{V}(t)$ is a monotonic increasing function of time t, with V(0) = 0, so the same trends will be observed when these functions are plotted against time t. Increasing Pe leads to increased final total throughput $V(t_f)$ and significant decreased initial average particle concentration in the filtrate $c_{avg}(0)$. Presumably this is because when Pe is small, the feed suspension transits the pleated membrane filter too rapidly due to the additional axial-pore diffusion effect, resulting in less total throughput and larger instantaneous averaged particle concentration remaining in the filtrate. However, for large values of Pe (the axial diffusion becomes mild and eventually ceases when $Pe \to \infty$), the slower feed suspension

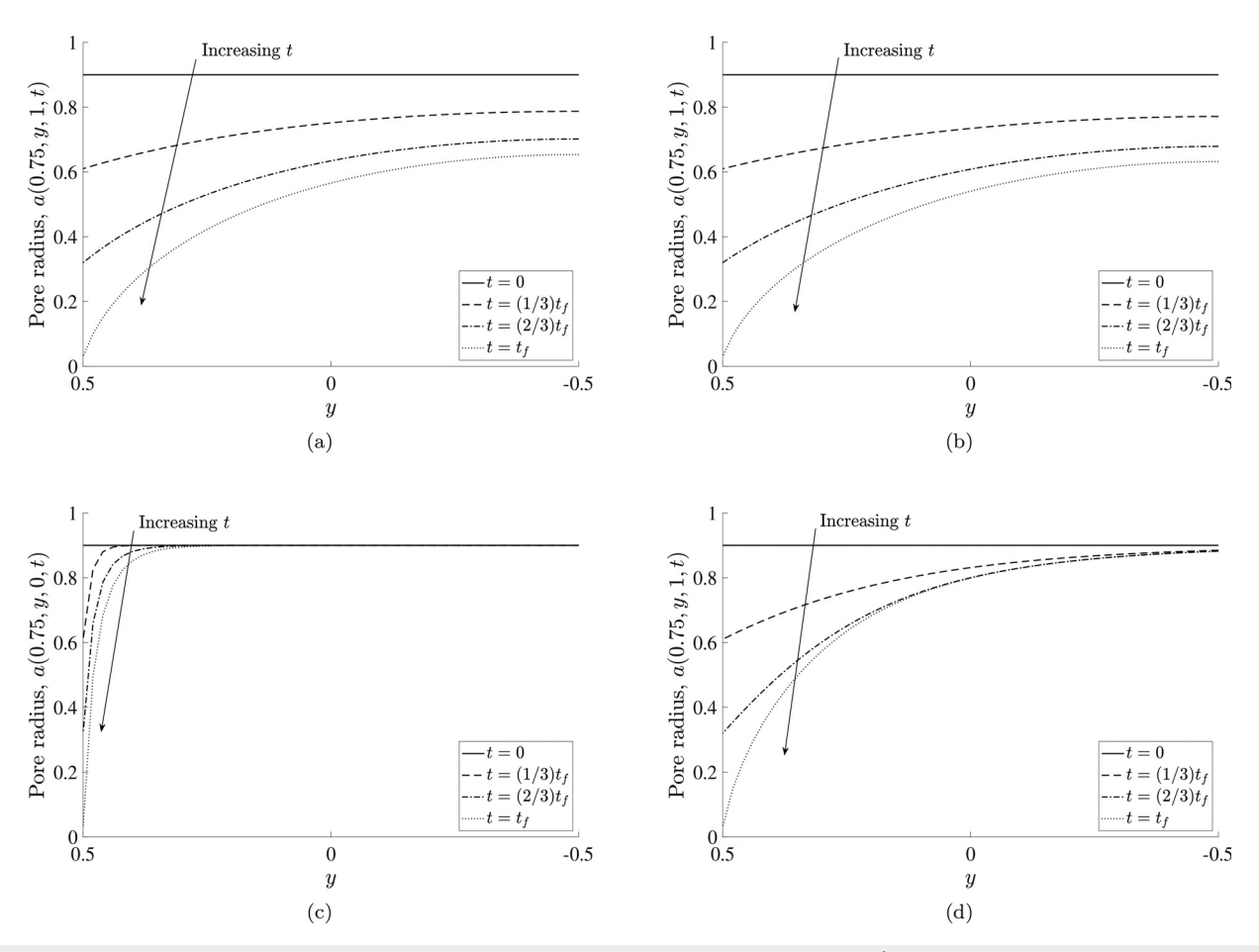


FIG. 2. Pore radius a(r,y,z,t) as a function of dimensionless pore length y, at selected times up to final time t_\hbar for $\mathcal{N}=90,~\Gamma=2.5,$ and k=2 at two selected locations for two values of Péclet number: (a) (r,z)=(0.75,0), top-center at the pleated membrane region and Pe =1, (b) (r,z)=(0.75,1), bottom-center in the pleated membrane region and Pe =1, (c) (r,z)=(0.75,0), top-center at the pleated membrane region and Pe =1, (c) =1, bottom-center in the pleated membrane region and Pe =1, (c) =1, bottom-center in the pleated membrane region and Pe =1, co. Other parameters are =1,

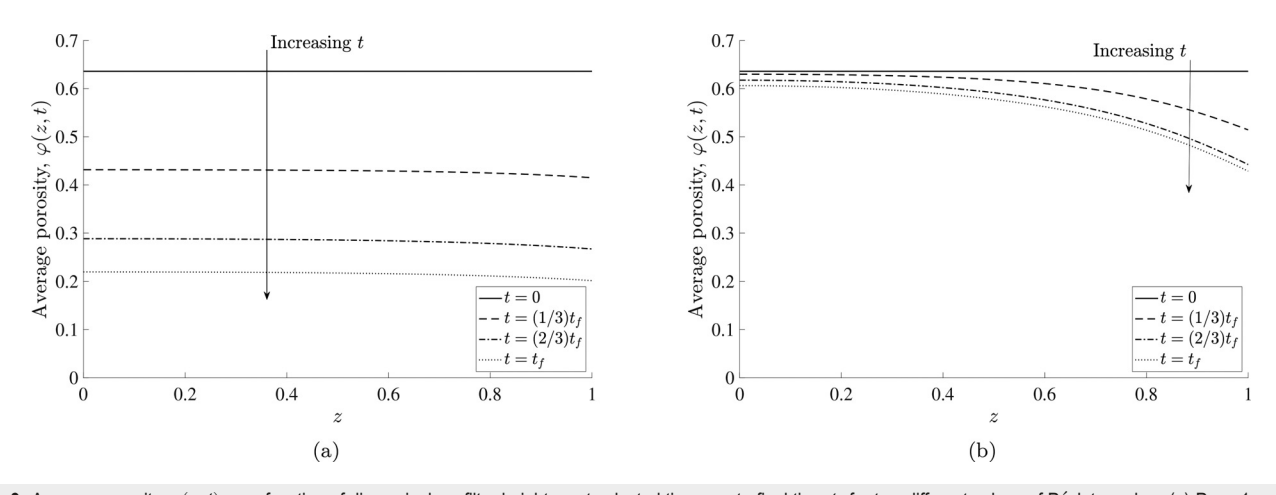
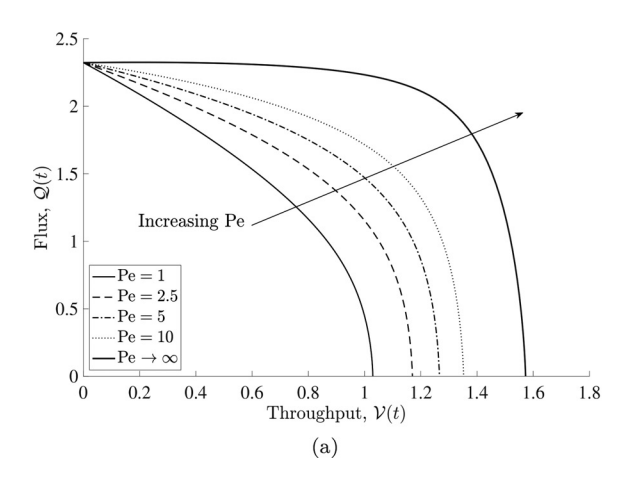


FIG. 3. Average porosity $\varphi(z,t)$ as a function of dimensionless filter height, z, at selected times up to final time t_{\hbar} for two different values of Péclet number: (a) Pe = 1 and (b) Pe $\rightarrow \infty$, with $\mathcal{N}=90, \ \Gamma=2.5$ and k=2. Other parameters are $d=0.5, l=0.5, \ \delta=0.1, \ \phi=0.5$, and $\lambda=2$.



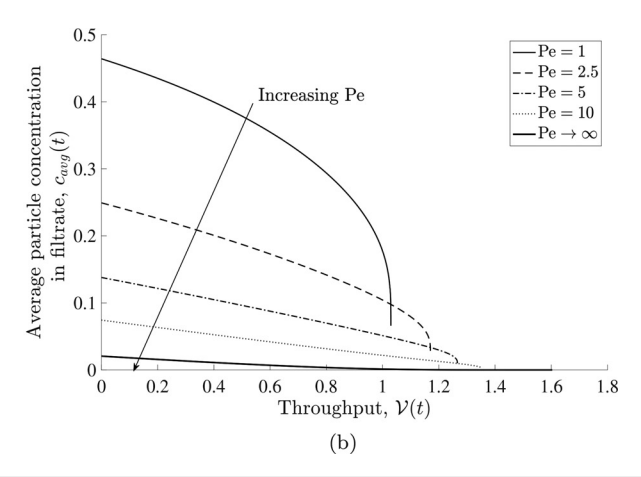


FIG. 4. Results for four different values of Péclet number Pe: (a) total flux $\mathcal{Q}(t)$ and (b) instantaneous averaged particle concentration in the filtrate $c_{avg}(t)$ as functions of throughput $\mathcal{V}(t)$, with $\mathcal{N}=90,\ \Gamma=2.5$, and k=2. Other parameters are $d=0.5,\ l=0.5,\ \delta=0.1,\ \phi=0.5$, and $\lambda=2$.

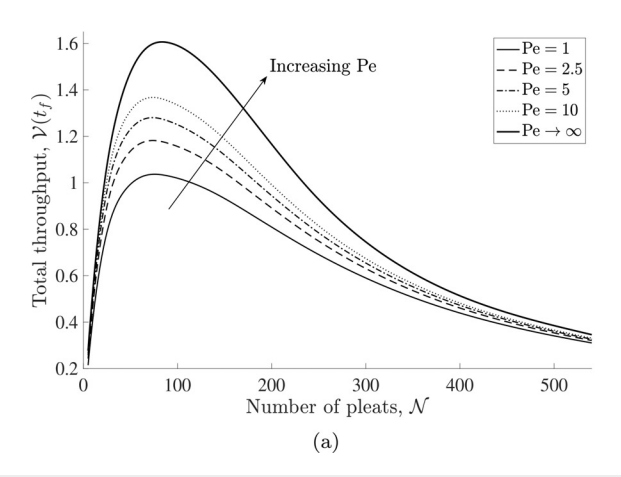
remains within the pleated membrane filter long enough to allow more particles adhere to the pores at a faster rate, causing quicker pore shrinkage at the upstream side [see Figs. 2(c) and 2(d)]. This could play an important role in the design of pleated membrane at the pore (micro) scale level.

The question every manufacturer wants answered is: What is the optimum pleat packing density that yields maximum performance while minimizing the energy required to operate the device (i.e., minimize the pressure drop)? For our model, this question translates to: What is the optimal number of pleats $\mathcal N$ that gives the maximum total throughput while maintains an acceptable initial average particle concentration in the filtrate? As shown in Table II, variation in θ_s affects three dimensionless parameters simultaneously: the number of pleats, $\mathcal N = \pi/\theta_s$; the dimensionless measure of the resistance of the packing material to that of the membrane, $\Gamma = (\pi R_m W^2)/(32K\theta_s D_m)$; and the dimensionless support layer permeability, $k = (180\theta_s)/\pi$. Recall that the permeability of the support layer is assumed to be constant in time; however, varying the pleat angle θ_s induces the change in the

permeability of the support layer spatially. We demonstrate the effect of pleat packing density by varying θ_s .

Figure 5 shows total throughput $\mathcal{V}(t_f)$ and initial average particle concentration in filtrate $c_{avg}(0)$ vs the total number of pleats \mathcal{N} for several different values of Pe. We find that an optimal total number of pleats \mathcal{N} exists that maximizes the total throughput $\mathcal{V}(t_f)$ for all values of Pe considered, as shown in Fig. 5(a). The presence of the maximum total throughput could be explained as follows: as the number of pleats \mathcal{N} is increased, there is a corresponding increase in the total surface area of the entire pleated membrane, which, in turns, leads to an increase in the total throughput and total system resistance as well. However, as we continue to increase the number of pleats \mathcal{N} the increased (pleated) supporting material imparts excessive filter resistance, tending to lower the total throughput. Thus, total throughput will eventually decrease once \mathcal{N} increases beyond a certain value.

In Fig. 5(b), we observe that the initial averaged particle concentration in filtrate $c_{avg}(0)$ decreases monotonically with \mathcal{N} . This makes sense for high pleat packing density filter, since most of the system



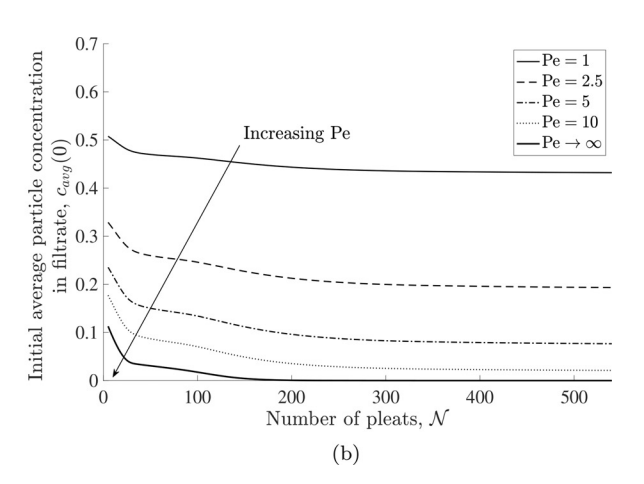


FIG. 5. (a) Total throughput $\mathcal{V}(t_f)$ and (b) initial averaged particle concentration in the filtrate $c_{avg}(0)$ as functions of the number of pleats, \mathcal{N} , for five different values of Péclet number Pe. Other parameters are d=0.5, l=0.5, $\delta=0.1$, $\phi=0.5$, and $\lambda=2$.

resistance comes from the porous support layers that surround the pleated membrane (see Fig. 1), increasing the total number of pleats $\mathcal N$ increases the amount of supporting material, which increases the flow resistance across the whole system and, hence, helps reduce the number of particles that can pass through the membrane. This figure also shows, for larger values of number of pleats $\mathcal N$ (over 200), the initial averaged particle concentration in the filtrate $c_{avg}(0)$ reaches steady state despite the values of Péclet number Pe. In other words, pleated filters with too high pleat packing density (PPD) are not efficient at least for removing the initial averaged particle in the filtrate. Note that as $\mathcal N \to \infty$, the dimensionless measure of the resistance of the packing material to that of the membrane $\Gamma \to \infty$ (see Table II), meaning that the membrane resistance is less compared to the packing material resistance; therefore, the membrane is not capable of removing additional particles.

In Fig. 6, we plot the total throughput as a function of the Péclet number Pe for three different values of $\mathcal N$. The results show that the total throughput increases as Pe increases for all values of $\mathcal N$ considered. For brevity of presentation, the results for the other values of $\mathcal N$ (which show the same trend) are not shown here. Observe that the total throughput is significantly higher when the PPD is neither too high (large $\mathcal N$) nor too low (small $\mathcal N$), suggesting that the PPD plays a very important role in the overall performance and the maximum throughput can be achieved when the value of $\mathcal N$ is intermediate. Note that $\mathcal N=76$ is the optimal value that maximizes the total throughput for finite values of Pe [see Fig. 5(a)].

VIII. CONCLUSIONS

In summary, we have used asymptotic methods to derive and analyze a mathematical model for fluid and particle transport in a pleated membrane filter. In particular, we have included the effects of particle axial-pore diffusion, pleated filter geometry, and pleat packing density to quantify the filtration performance in pleated filters, which were not considered in previous studies. ^{29,30,32,34}

Throughout our analysis, the focus has been on the design of pleated membrane filters. This included (i) understanding how the membrane internal pore structure and morphology affect the filter performance under certain operating conditions and (ii) expressions to

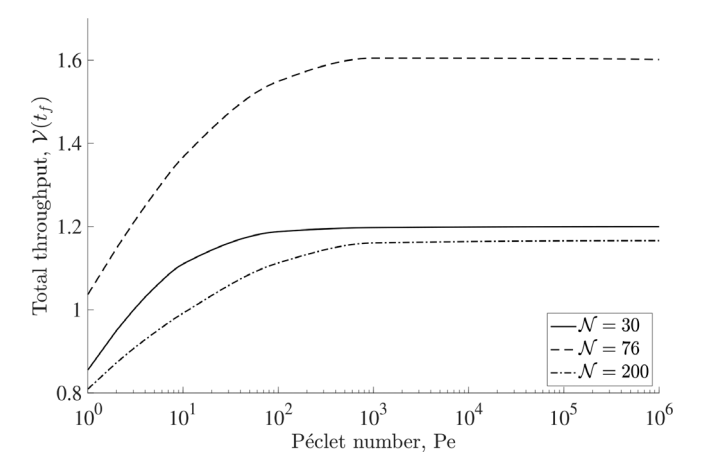


FIG. 6. Total throughput $\mathcal{V}(t_f)$ as a function of the Péclet number Pe for three different values of \mathcal{N} . Other parameters are d=0.5, l=0.5, $\delta=0.1$, $\phi=0.5$, and $\lambda=2$.

relate the desired pleat packing density (in our model, the optimal range of numbers of pleats) that optimize the performance in terms of total throughput while maintaining an acceptable level of particle retention.

Our results in Figs. 2(c) and 2(d) show that for the filtration process operating under a high Péclet number regime, the membrane pore closure mainly occurs at the upstream side, while the rest of pore remains minimally used. This means that in real applications, we must discard and replace the membrane, even if a large proportion of the membrane remains unused. Hence, it is efficient to have a membrane structure resulting in a uniform final porosity or pore profile, meaning that most part of the filter is being used to remove particles. Therefore, we can conclude that for the design of pleated membrane filters operating under high Péclet numbers, the membrane pores should be wider at the upstream side to allow this area of the pore to have removed more particles.

The results of our investigation in Fig. 5 indicate that changing the number of pleats (pleat packing density) appears to have a significant impact on the overall performance and operating cost (more total throughput and less energy used in the filtration process). Specifically, we found that by increasing the number of pleats, the total throughput in the final filtration process also increases. However, a very large number of pleats packed in the pleated filter (corresponds to very high pleat packing density) will inhibit the total throughput due to excessive resistance stemming from the overly packed support layers.

The model we have presented should be useful in the future design of pleated filter membranes and offers a deeper understanding of the filtration process in these filters; however, we have made several simplifying assumptions and are open to improvement in a number of areas. First, the particle transport is simplified compared to real-world filtration scenarios. In most applications, particle transport generally involves complex variable diffusion coefficients such as non-uniform flow field and spatially variable diffusion. Although it is frequently modeled using the constant diffusion coefficient, it would be interesting and highly relevant to extend the current framework to capture these features. Second, the fouling mechanism considered in this work is adequate to capture standard adsorptive fouling. Our model can be readily expanded to a generalized one to allow for multiple fouling mechanisms (see, for example, the work by Sanaei and Cummings⁵). Finally, the current membrane morphology (pore structure and connectivity) is modeled using a series of initial identical cylindrical pores, and there are more complex morphologies that could be included in our model (see, for example, the work by Gu et al., 43 Griffiths et al., 5 and Sanaei and Cummings⁵¹).

ACKNOWLEDGMENTS

P.S. is supported by an Institutional Support of Research and Creativity (ISRC) Grant provided by New York Institute of Technology and financial support from the National Science Foundation (NSF) under Grant No. DMS-2108161. The views expressed in this article are D. Fong's own and not those of the U.S. Merchant Marine Academy, the Maritime Administration, the Department of Transportation, or the United States government.

AUTHOR DECLARATIONS Conflict of Interest

The authors have no conflicts to disclose.

Author Contributions

Daniel Fong: Conceptualization (equal); Formal analysis (equal); Software (equal); Validation (equal); Visualization (equal); Writing – original draft (equal); Writing – review & editing (equal). Pejman Sanaei: Conceptualization (equal); Formal analysis (equal); Funding acquisition (equal); Investigation (equal); Methodology (equal); Project administration (equal); Resources (equal); Software (equal); Validation (equal); Visualization (equal); Writing – original draft (equal); Writing – review & editing (equal).

DATA AVAILABILITY

The data that support the findings of this study are available from the corresponding author upon reasonable request.

REFERENCES

- ¹E. Iritani, "A review on modeling of pore-blocking behaviors of membranes during pressurized membrane filtration," Drying Technol. 31, 146–162 (2013).
- ²C.-C. Ho and A. L. Zydney, "A combined pore blockage and cake filtration model for protein fouling during microfiltration," J. Colloid Interface Sci. 232, 389–399 (2000).
- ³P. Sanaei and L. J. Cummings, "Flow and fouling in membrane filters: Effects of membrane morphology," J. Fluid Mech. **818**, 744–771 (2017).
- ⁴M. P. Dalwadi, M. Bruna, and I. M. Griffiths, "A multiscale method to calculate filter blockage," J. Fluid Mech. 809, 264–289 (2016).
- ⁵P. Sanaei and L. J. Cummings, "Membrane filtration with multiple fouling mechanisms," Phys. Rev. Fluids 4, 124301 (2019).
- ⁶D. Fong, L. Cummings, S. Chapman, and P. Sanaei, "On the performance of multilayered membrane filters," J. Eng. Math. **127**, 23 (2021).
- ⁷M. P. Dalwadi, I. M. Griffiths, and M. Bruna, "Understanding how porosity gradients can make a better filter using homogenization theory," Proc. R. Soc. A 471, 20150464 (2015).
- ⁸I. Griffiths, A. Kumar, and P. Stewart, "A combined network model for membrane fouling," J. Colloid Interface Sci. **432**, 10–18 (2014).
- ⁹G. Bolton, D. LaCasse, and R. Kuriyel, "Combined models of membrane fouling: Development and application to microfiltration and ultrafiltration of biological fluids," J. Membr. Sci. 277, 75–84 (2006).
- ¹⁰G. R. Bolton, A. W. Boesch, and M. J. Lazzara, "The effects of flow rate on membrane capacity: Development and application of adsorptive membrane fouling models," J. Membr. Sci. 279, 625–634 (2006).
- ¹¹C.-C. Ho and A. L. Zydney, "Effect of membrane morphology on the initial rate of protein fouling during microfiltration," J. Membr. Sci. 155, 261–275 (1999).
- ¹²H. Lonsdale, "The growth of membrane technology," J. Membr. Sci. 10, 81–181 (1982).
- ¹³S. Roy, "Innovative use of membrane technology in mitigation of GHG emission and energy generation," Procedia Environ. Sci. 35, 474–482 (2016).
- ¹⁴R. Van der Sman, H. Vollebregt, A. Mepschen, and T. Noordman, "Review of hypotheses for fouling during beer clarification using membranes," J. Membr. Sci. 396, 22–31 (2012).
- ¹⁵L. Fillaudeau and H. Carrère, "Yeast cells, beer composition and mean pore diameter impacts on fouling and retention during cross-flow filtration of beer with ceramic membranes," J. Membr. Sci. 196, 39–57 (2002).
- ¹⁶C. Bhattacharjee, V. Saxena, and S. Dutta, "Fruit juice processing using membrane technology: A review," Innovative Food Sci. Emerg. Technol. 43, 136–153 (2017).
- ¹⁷J. Monte, M. Sá, C. Parreira, J. Galante, A. R. Serra, C. F. Galinha, L. Costa, V. J. Pereira, C. Brazinha, and J. G. Crespo, "Recycling of dunaliella salina cultivation medium by integrated membrane filtration and advanced oxidation," Algal Res. 39, 101460 (2019).
- ¹⁸S. Munirasu, M. A. Haija, and F. Banat, "Use of membrane technology for oil field and refinery produced water treatment? A review," Process Saf. Environ. Prot. 100, 183–202 (2016).

- ¹⁹M. Y. Li, D. Chin, C. Puelz, and P. Sanaei, "Simulating liquid-gas interfaces and moving contact lines with the immersed boundary method," Phys. Fluids 34, 053323 (2022).
- ²⁰B. Santos, J. G. Crespo, M. A. Santos, and S. Velizarov, "Oil refinery hazardous effluents minimization by membrane filtration: An on-site pilot plant study," J. Environ. Manag. 181, 762–769 (2016).
- ²¹I. Khouni, G. Louhichi, A. Ghrabi, and P. Moulin, "Efficiency of a coagulation/flocculation-membrane filtration hybrid process for the treatment of vegetable oil refinery wastewater for safe reuse and recovery," Process Saf. Environ. Prot. 135, 323–341 (2020).
- ²²M. Gryta, K. Karakulski, and A. Morawski, "Purification of oily wastewater by hybrid UF/MD," Water Res. 35, 3665–3669 (2001).
- ²³R. van Reis and A. Zydney, "Bioprocess membrane technology," J. Membr. Sci. 297, 16–50 (2007).
- ²⁴A. Polidori, P. Fine, V. White, and P. Kwon, "Pilot study of high-performance air filtration for classroom applications," <u>Indoor Air</u> 23, 185–195 (2013).
- ²⁵B. C. Smith, B. C. Ramirez, S. J. Hoff, J. D. Harmon, and J. P. Stinn, "Design and validation of a mobile laboratory for testing air inlet filter loading at animal houses," Agric. Eng. Int.: CIGR J. 21, 39 (2019).
- ²⁶C. Ricketts and P. Smith, "A model for the stresses in the filter medium of deep-pleat HEPA-filter packs: Implications and applications in review," in 28th Nuclear Air Cleaning Conference (2004), Vol. 8.
- ²⁷C. He, C. Yan, C. Tang, M. Huang, L. Ren, and M. Zhang, "Nitrogen pulse jet cleaning of the pleated filter cartridge clogged with adhesive hygroscopic dusts," Process Saf. Environ. Prot. 147, 430–438 (2021).
- ²⁸F. Meng, S.-R. Chae, A. Drews, M. Kraume, H.-S. Shin, and F. Yang, "Recent advances in membrane bioreactors (MBRs): Membrane fouling and membrane material," Water Res. 43, 1489–1512 (2009).
- ²⁹Y. Sun, P. Sanaei, L. Kondic, and L. J. Cummings, "Modeling and design optimization for pleated membrane filters," Phys. Rev. Fluids 5, 044306 (2020).
- ³⁰D. Persaud, M. Smirnov, D. Fong, and P. Sanaei, "Modeling of the effects of pleat packing density and cartridge geometry on the performance of pleated membrane filters," Fluids 6, 209 (2021).
- ³¹C. Da-Ren and D. Y. Pui, "Optimization of pleated filter designs using a finiteelement numerical model," J. Aerosol Sci. 23, 579–590 (1996).
- ³²P. Sanaei, G. Richardson, T. Witelski, and L. Cummings, "Flow and fouling in a pleated membrane filter," J. Fluid Mech. **795**, 36–59 (2016).
- ³³A. I. Brown, "An ultra scale-down approach to the rapid evaluation of pleated membrane cartridge filter performance," Ph.D. thesis (University College London, 2011).
- ³⁴V. E. Pereira, M. P. Dalwadi, E. Ruiz-Trejo, and I. M. Griffiths, "Optimising the flow through a concertinaed filtration membrane," J. Fluid Mech. 913, A28 (2021).
- ³⁵G. I. Taylor, "Dispersion of soluble matter in solvent flowing slowly through a tube," Proc. R. Soc. London, Ser. A 219, 186–203 (1953).
- ³⁶S. Y. Liu, Z. Chen, and P. Sanaei, "Effects of particles diffusion on membrane filters performance," Fluids 5, 121 (2020).
- 37I. Griffiths, P. Howell, and R. Shipley, "Control and optimization of solute transport in a thin porous tube," Phys. Fluids 25, 033101 (2013).
- ³⁸G. S. Beavers and D. D. Joseph, "Boundary conditions at a naturally permeable wall," J. Fluid Mech. 30, 197–207 (1967).
- ³⁹S. Hahn, J. Je, and H. Choi, "Direct numerical simulation of turbulent channel flow with permeable walls," J. Fluid Mech. 450, 259–285 (2002).
- ⁴⁰M. Sahraoui and M. Kaviany, "Slip and no-slip velocity boundary conditions at interface of porous, plain media," Int. J. Heat Mass Transfer 35, 927–943
- 41P. G. Saffman, "On the boundary condition at the surface of a porous medium," Stud. Appl. Math. 50, 93–101 (1971).
- ⁴²R. F. Probstein, *Physicochemical Hydrodynamics: An Introduction* (John Wiley & Sons, 2005).
- ⁴³B. Gu, D. Renaud, P. Sanaei, L. Kondic, and L. Cummings, "On the influence of pore connectivity on performance of membrane filters," J. Fluid Mech. 902, A5 (2020).
- 44P. Sanaei, L. Cummings, S. Waters, and I. Griffiths, "Curvature-and fluid-stress-driven tissue growth in a tissue-engineering scaffold pore," Biomech. Model. Mechanobiol. 18, 589–605 (2019).

- ⁴⁵Z. Chen, S. Y. Liu, I. C. Christov, and P. Sanaei, "Flow and fouling in elastic membrane filters with hierarchical branching pore morphology," Phys. Fluids 33, 062009 (2021).
- 46 L.-M. Lo, S.-C. Hu, D.-R. Chen, and D. Y. Pui, "Numerical study of pleated fabric cartridges during pulse-jet cleaning," Powder Technol. 198, 75–81 (2010).
- (2010).

 47 A. Waghode, N. Hanspal, R. Wakeman, and V. Nassehi, "Numerical analysis of medium compression and losses in filtration area in pleated membrane cartridge filters," Chem. Eng. Commun. 194, 1053-1064 (2007).
- ⁴⁸R. Wakeman, N. Hanspal, A. Waghode, and V. Nassehi, "Analysis of pleat crowding and medium compression in pleated cartridge filters," Chem. Eng. Res. Des. 83, 1246–1255 (2005).
- ⁴⁹N. B. Jackson, M. Bakhshayeshi, A. L. Zydney, A. Mehta, R. van Reis, and R. Kuriyel, "Internal virus polarization model for virus retention by the Ultipor® VF Grade DV20 membrane," <u>Biotechnol. Prog.</u> 30, 856–863 (2014).
- 50I. Griffiths, A. Kumar, and P. Stewart, "Designing asymmetric multilayered membrane filters with improved performance," J. Membr. Sci. 511, 108–118 (2016).
- ⁵¹P. Sanaei and L. J. Cummings, "Membrane filtration with complex branching pore morphology," Phys. Rev. Fluids 3, 094305 (2018).